NeuroImage 129 (2016) 133–147

Contents lists available at ScienceDirect

NeuroImage

journal homepage: www.elsevier.com/locate/ynimg

Automatic EEG-assisted retrospective motion correction for fMRI (aE-REMCOR)

Chung-Ki Wong [a], Vadim Zotev [a], Masaya Misaki [a], Raquel Phillips [a], Qingfei Luo [a], Jerzy Bodurka [a,b,c,*]

[a] Laureate Institute for Brain Research, Tulsa, OK, USA
[b] College of Engineering, University of Oklahoma, Norman, OK, USA
[c] Center for Biomedical Engineering, University of Oklahoma, Norman, OK, USA

ARTICLE INFO

Article history:
Received 1 September 2015
Accepted 20 January 2016
Available online 27 January 2016

Keywords:
Motion correction
Motion artifacts
E-REMCOR
fMRI
EEG
EEG-fMRI
ICA

ABSTRACT

Head motions during functional magnetic resonance imaging (fMRI) impair fMRI data quality and introduce systematic artifacts that can affect interpretation of fMRI results. Electroencephalography (EEG) recordings performed simultaneously with fMRI provide high-temporal-resolution information about ongoing brain activity as well as head movements. Recently, an EEG-assisted retrospective motion correction (E-REMCOR) method was introduced. E-REMCOR utilizes EEG motion artifacts to correct the effects of head movements in simultaneously acquired fMRI data on a slice-by-slice basis. While E-REMCOR is an efficient motion correction approach, it involves an independent component analysis (ICA) of the EEG data and identification of motion-related ICs. Here we report an automated implementation of E-REMCOR, referred to as aE-REMCOR, which we developed to facilitate the application of E-REMCOR in large-scale EEG-fMRI studies. The aE-REMCOR algorithm, implemented in MATLAB, enables an automated preprocessing of the EEG data, an ICA decomposition, and, importantly, an automatic identification of motion-related ICs. aE-REMCOR has been used to perform retrospective motion correction for 305 fMRI datasets from 16 subjects, who participated in EEG-fMRI experiments conducted on a 3 T MRI scanner. Performance of aE-REMCOR has been evaluated based on improvement in temporal signal-to-noise ratio (TSNR) of the fMRI data, as well as correction efficiency defined in terms of spike reduction in fMRI motion parameters. The results show that aE-REMCOR is capable of substantially reducing head motion artifacts in fMRI data. In particular, when there are significant rapid head movements during the scan, a large TSNR improvement and high correction efficiency can be achieved. Depending on a subject's motion, an average TSNR improvement over the brain upon the application of aE-REMCOR can be as high as 27%, with top ten percent of the TSNR improvement values exceeding 55%. The average correction efficiency over the 305 fMRI scans is 18% and the largest achieved efficiency is 71%. The utility of aE-REMCOR on the resting state fMRI connectivity of the default mode network is also examined. The motion-induced position-dependent error in the DMN connectivity analysis is shown to be reduced when aE-REMCOR is utilized. These results demonstrate that aE-REMCOR can be conveniently and efficiently used to improve fMRI motion correction in large clinical EEG-fMRI studies.

Introduction

Head motion has been recognized as a major source of artifacts in fMRI data since early days of fMRI (e.g. Cox and Hyde, 1997; Friston et al., 1995, 1996; Hajnal et al., 1994; Jiang et al., 1995). In task fMRI, motion-induced artifacts often correlate with experimental tasks (Hajnal et al., 1994), leading to inaccurate estimates of BOLD activity levels and reduced significance of fMRI findings. This issue is particularly important for frontal and prefrontal brain regions that usually exhibit the largest motions. In resting-state fMRI, head movements introduce systematic changes in estimated fMRI functional connectivity strength across the brain (Power et al., 2012; Van Dijk et al., 2012). Such spurious changes can lead to incorrect interpretations of the functional connectivity results on the group level if the data is ineffectively preprocessed (Power et al., 2012; Saad et al., 2013; Gotts et al., 2013; Jo et al., 2013). The traditional fMRI motion correction approach bases on spatial co-registration of 3D fMRI volumes (e.g. Friston et al., 1995; Cox and Jesmanowicz, 1999). Despiking at the beginning of the preprocessing pipeline further attenuates the fMRI motion effect (Jo et al., 2013; Satterthwaite et al., 2013). The traditional approach implicitly assumes that all motion occurs between the volume acquisitions (Cox and Hyde, 1997). Thus, it cannot adequately take into account effects of faster intra-volume movements (Beall and Lowe, 2014). It has been suggested that a slice-based fMRI motion correction can be superior to the

* Corresponding author at: Laureate Institute for Brain Research, Tulsa, OK, USA.
E-mail address: jbodurka@laureateinstitute.org (J. Bodurka).

http://dx.doi.org/10.1016/j.neuroimage.2016.01.042

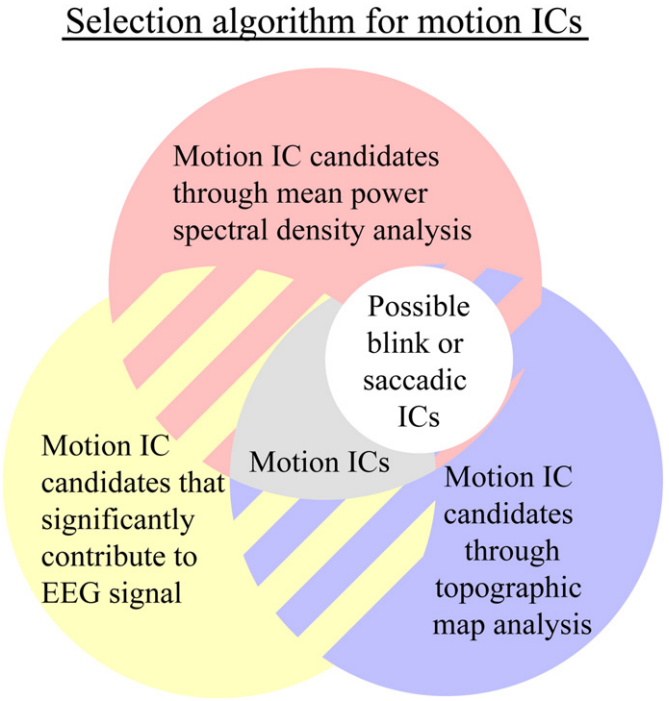

Fig. 1. The sketch of the automatic identification of ICs through the analyses of the mean power spectral density, topographic map, and contribution to the EEG signal. Possible blink and saccade ICs are removed from the motion ICs selection.

traditional volume registration approach (Beall and Lowe, 2014; Zotev et al., 2012).

Multimodal brain imaging, combining fMRI with simultaneous EEG recordings (e.g. Mulert and Lemieux, 2010), offers new exciting opportunities for fMRI motion correction. Simultaneous EEG-fMRI combines the advantages of the high temporal resolution of EEG and the high spatial resolution of fMRI. While the artifact on the fMRI data can be minimized with the use of MR-compatible EEG system, introduction of fMRI environment related artifacts to the EEG data is inevitable. In particular, cardioballistic and motion artifacts are exacerbated inside an MR scanner. These artifacts can be reduced with designated hardware setup (Bonmassar et al., 2002; Masterton et al., 2007), or corrected effectively by independent component analysis (Srivastava et al., 2005; Mantini et al., 2007).

Recently, we introduced a method for EEG-assisted retrospective motion correction of fMRI data (E-REMCOR) that employs the EEG array as a sensitive motion detector in addition to recording neuronal activity (Zotev et al., 2012). In this method, voltage artifacts induced in the EEG array leads due to head motion in a strong uniform magnetic field of an MRI scanner are used to define regressors describing rotational head movements with millisecond temporal resolution. E-REMCOR makes it possible to regress out the effects of rapid head movements from unprocessed fMRI data on a slice-by-slice basis prior to volume registration. Thus, E-REMCOR complements both the traditional fMRI volume registration approach, which performs better for slower head motions, and the RETROICOR method for slice-specific correction of fMRI cardiorespiratory artifacts (Glover et al., 2000). E-REMCOR does not require any specialized equipment (beyond the EEG-fMRI instrumentation) and can be applied retrospectively to any existing EEG-fMRI dataset.

Application of E-REMCOR involves an independent component analysis (ICA) of EEG data and identification of independent components (ICs) corresponding to different head motions. This process requires a close examination of the EEG recordings and a careful evaluation of the IC properties. Therefore, an automation of E-REMCOR to enable a robust and efficient motion correction without human supervision is desirable. In this paper, we describe such an automation extension of E-REMCOR, which we refer to as aE-REMCOR. We explicitly detail the quantitative criteria that effectively distinguish the different motion ICs. We also evaluate its performance for a large number of EEG-fMRI datasets. An improved automatic fMRI motion correction afforded by aE-REMCOR would provide an additional incentive for recording EEG during fMRI, and thus encourage a broader use of simultaneous EEG-fMRI. It would also greatly benefit large clinical studies by improving fMRI data quality and reducing numbers of subjects excluded due to excessive motion.

Methods

E-REMCOR

The aE-REMCOR method is an automation extension of E-REMCOR. E-REMCOR is based on the observation that voltage artifacts (electromotive force, EMF) induced in EEG leads due to rigid-body movements of the head in the uniform magnetic field of an MRI scanner can be analytically related to time derivatives of real-time rotational head motion parameters (Zotev et al., 2012). Definition of the high-temporal-resolution E-REMCOR regressors is independent of the fMRI pulse sequence properties. The MR artifacts are removed from the EEG data by means of the average artifact subtraction (Allen et al., 2000) before the EEG data are used for E-REMCOR.

Application of E-REMCOR for fMRI motion correction includes three steps. First, an independent component analysis (ICA, e.g. Bell and Sejnowski, 1995; Makeig et al., 1997) is performed for the EEG data:

$$V_i(t) = \sum_{j=1}^{N} b_{ij} F_j(t) + \varepsilon_i(t), \quad i = 1...N. \tag{1}$$

Here, $\{V_i(t)\}$ are signals from N EEG channels, $\{F_j(t)\}$ are the corresponding independent components (ICs), $\{b_{ij}\}$ are elements of the ICA back-projection matrix, and $\varepsilon_i(t)$ is an error term also including the ith-channel's Gaussian noise The ICs $F_k(t)$, $k = 1...K$, approximating random-motion and/or cardioballistic (CB) artifacts $V_{\mathrm{EMF}}^{(i)}(t)$ are

$$V_{\mathrm{EMF}}^{(i)}(t) \approx \sum_{k=1}^{K} b_{ik} F_k(t), \quad i = 1...N, K \le N. \tag{2}$$

The identification criteria for the random head motion are outlined in Zotev et al., 2012. The quantitative classification of the criteria for the random head motion, together with the cardioballistic motions caused by cardiac pulsations, will be detailed in the following sections.

Second, each motion-related IC $F_k(t)$ is band-pass filtered from 0.1 to 20 Hz and integrated over time (with constant $\Delta t = 0.4$ s) to yield two E-REMCOR regressors, $R_1^{(k)}(t)$ and $R_2^{(k)}(t)$, having the same temporal

Fig. 2. (a)–(f) The mean power spectral density of (a) a rapid head movement IC; (b) a cardioballistic motion IC; (c) a mixture of cardioballistic motion and rapid head movement IC; (d) another rapid head movement IC with reflection points in the RM range; (e) a blink IC; (f) a saccade IC. (g)–(h): The rises of peaks B and E in (c) from their neighboring left and right minima when the neighboring right minimum is below 8 Hz. (i)–(j): The rises of the NR peaks G and K in (c) and (e). (k): The rise of the reflection points in (d). In (a)–(f), S_0 is the difference between the maximum and minimum spectrum power below 4 Hz. Motion frequency range (MO) refers to the combined frequency range of RM and CB. RM, CB and MO peaks stand for the peaks found in the RM, CB and MO frequency ranges respectively. In (g)–(h), the peak rise is defined as the average of the left and right rises. In (i), the peak rise is the power difference between the peak G and the minimum between F and G. In (j), the peak rise is the power difference between the peak K and the minimum value between J and K. In (k), the rise of the reflection point H is the power difference between H and I, and the rise of the reflection point I is the power difference between I and $S(\nu = 4.5$ Hz).

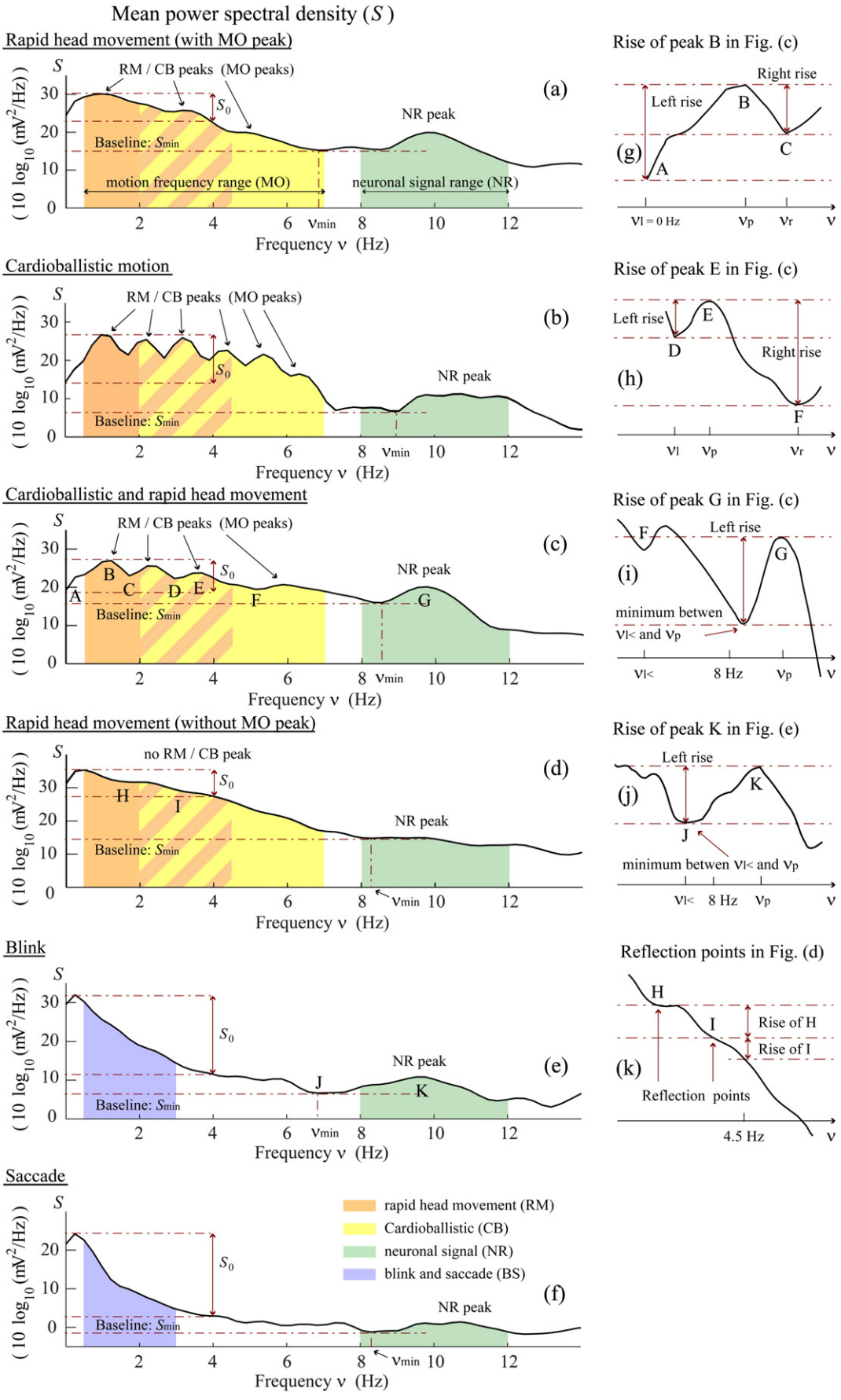
Mean power spectral density (S)
Rapid head movement (with MO peak)
RM / CB peaks (MO peaks)
NR peak
Baseline: Smin
motion frequency range (MO)
neuronal signal range (NR)
(a)
Cardioballistic motion
(b)
Cardioballistic and rapid head movement
(c)
Rapid head movement (without MO peak)
no RM / CB peak
(d)
Blink
(e)
Saccade
(f)
Frequency ν (Hz)
rapid head movement (RM)
Cardioballistic (CB)
neuronal signal (NR)
blink and saccade (BS)
Rise of peak B in Fig. (c)
Left rise
Right rise
(g)
Rise of peak E in Fig. (c)
(h)
Rise of peak G in Fig. (c)
minimum betwen
(i)
Rise of peak K in Fig. (e)
(j)
Reflection points in Fig. (d)
Rise of H
Rise of I
Reflection points
(k)
4.5 Hz

resolution as the EEG data:

$$R_1^{(k)}(t) = \int_{t-\Delta t}^{t} F_k(\tau)d\tau, \text{ and } R_2^{(k)}(t) = \int_{0}^{t-\Delta t} F_k(\tau)d\tau. \quad (3)$$

Third, the E-REMCOR regressors are sub-sampled to match the acquisition times $\{t_s\}$ for each slice in the fMRI dataset and linearly detrended. Correction of motion artifacts in the unprocessed fMRI data is performed by means of a linear regression procedure (with fit coefficients $\{\beta\}$ and a linear regressor R_L) applied to each fMRI voxel's time course:

$$S_{fMRI}(t_s) = \beta_0 + \beta_1 R_L(t_s) + \sum_{k=1}^{K}\left[\beta_{k1}R_1^{(k)}(t_s) + \beta_{k2}R_2^{(k)}(t_s)\right] + \varepsilon(t_s). \quad (4)$$

Thus, the E-REMCOR motion correction is performed on a slice-by-slice basis, and can be applied simultaneously with RETROICOR. It is usually followed by the standard fMRI data processing with slice-time adjustment and volume registration to correct effects of slower head motions.

The purpose of aE-REMCOR is to automate and streamline the practical use of E-REMCOR for large datasets and/or groups of subjects. We developed an advanced algorithm for automatic identification of motion-related ICs, Eq. (2). The algorithm automatically characterizes and recognizes the special features of the motion artifacts imposed on the mean power spectral density, topographic map, and EEG signal contribution of the ICs as described in detail below. In the previous work, the motion ICs were prepared with Brain Products, GmbH's Analyzer 2 proprietary software. The current automation procedure is implemented in MATLAB, together with the MR artifact removal, the ICA decomposition, and the IC integration, Eq. (3). The final motion correction step, Eq. (4), is performed for fMRI data in AFNI (Cox, 1996; Cox and Hyde, 1997) using the 3dTfitter AFNI program.

Data acquisition

The study was conducted at the Laureate Institute for Brain Research. The research protocol was approved by the Western Institutional Review Board (IRB). Eleven PTSD patients and five healthy controls (mean age 31 ± 8 years, all male) participated in the study. The study included three EEG-fMRI scanning sessions. Each session lasted for about two hours and was separated approximately one week apart. In each session, there were five real time fMRI neurofeedback (rtfMRI-nf) training scans (Zotev et al., 2011) and two resting scans immediately before and after the rtfMRI-nf training scans. In this study, the scans with missing fMRI slice markers, or mismatched EEG and fMRI scan numbers were not considered, giving a total of 305 scans in the analysis, which includes 219 rtfMRI-nf training scans and 86 resting scans.

The experimental procedure and data acquisition parameters were the same as described in Zotev et al., 2012. The EEG-fMRI experiments were conducted on a GE Discovery MR750 3 T MRI scanner with a standard 8-channel receive-only head coil. A single-shot gradient-echo EPI sequence with Sensitivity Encoding (SENSE) was employed for fMRI. The following EPI imaging parameters were used: repetition time $TR = 2000$ ms, echo time $TE = 30$ ms, FOV = 240 mm, 34 axial slices per volume, slice thickness = 2.9 mm, slice gap = 0.5 mm, 96 × 96 acquisition matrix, SENSE acceleration factor $R = 2$, flip angle = 90°, sampling bandwidth = 250 kHz. Each fMRI run lasted 8 min 46 s. Three EPI volumes (6 s) were excluded from the data analysis to allow the fMRI signal to reach steady state. The EPI images were reconstructed into a 128 × 128 matrix, so the resulting fMRI voxel size was 1.875 × 1.875 × 2.9 mm^3. Physiological pulse oximetry and respiration waveforms were also simultaneously acquired with fMRI. The EEG recordings were performed simultaneously with fMRI using a 32-channel MR-compatible EEG system from Brain Products GmbH. The EEG signals were acquired with 16-bit 5 kS/s sampling providing 0.2 ms temporal and 0.1 μV measurement resolution. The signals were measured relative to the standard reference (FCz) and were hardware-filtered between 0.016 Hz (10 s time constant) and 250 Hz during the acquisition.

EEG preprocessing and ICA

The EEG data, together with the information about event markers and MRI slice markers, are loaded in MATLAB using the EEGLAB (Delorme and Makeig, 2004) command pop_loadbv(). The MRI slice markers are used to label the time period of the concurrent EEG and fMRI measurements. Because the MR artifacts are strictly periodic with the fMRI repetition time *TR*, they are efficiently removed from the EEG data using the average artifact subtraction. The EEG data are then low-pass filtered at 40 Hz and downsampled to 250 S/s (4 ms sampling interval). Band-rejection filters (1 Hz bandwidth) are applied to remove harmonics of the fMRI slice selection frequency, 17 Hz, as well as the AC power line artifact at 60 Hz, and a vibration artifact at 26 Hz.

The ICA is performed on the preprocessed EEG data using the Informax algorithm (Bell and Sejnowski, 1995) implemented in EEGLAB (binica, Delorme and Makeig, 2004) to separate 31 ICs for $N = 31$ EEG channels. The ICs related to head motions, Eq. (2), are identified automatically. The selected ICs are bandpass filtered from 0.1 to 20 Hz to exclude both the slowly and fast varying contributions that may be unrelated to head motion (such as EEG instrumentation drifts). The ICs are then used to define E-REMCOR regressors, Eq. (3).

Automatic identification of motion ICs

In aE-REMCOR, the ICs corresponding to head motions are identified automatically. An IC is recognized as motion-related if its mean power spectral density, topographic map, and contribution to the EEG signal manifest certain features that are generally observed for motion ICs. Note that our original work on E-REMCOR focused on correction of artifacts corresponding to random head movements so CB artifacts were removed from the EEG data using the average artifact subtraction (Allen et al., 1998). In the present paper, the CB artifacts are included in the analysis together with the random-motion artifacts. The reason is that a certain type of head motion can contribute to both random and cardioballistic head movements, so the two kinds of artifacts are not entirely independent and may be hard to separate (Zotev et al., 2012). The inclusion of CB artifacts makes the E-REMCOR procedure more flexible, but it does not, in general, eliminate the need for RETROICOR.

The aE-REMCOR automation algorithm is illustrated in Fig. 1. ICs related to rapid head motion and cardioballistic motions are recognized when the criteria in the analyses of mean power spectral density, topographic map, and EEG signal contribution are simultaneously satisfied. Eye blink ICs and saccadic ICs are also identified in addition to the head motion ICs to ensure proper separation of head movement and eye movement artifacts. The IC classification parameters used in this paper are determined empirically across 305 EEG-fMRI scans from 16 subjects. The three sections below describe the quantification of the characteristics and the identification of the motion ICs through the analyses of mean power spectral density (Section 2.5), topographic map (Section 2.6), and EEG signal contribution (Section 2.7).

Motion IC identification through power spectral density analysis

To better understand the physical origins of the ICs, the mean power spectral density of each IC is analyzed. In aE-REMCOR, the mean power spectral density (S) is computed using the MATLAB function pwelch() over time windows of 2.048 s length with 1.024 s overlap (512 and 256 data points with 4 ms sampling). The spectral resolution ($\Delta\nu$) is 0.244 Hz. Fig.2 shows some typical spectra for the ICs related to motions, blink and saccade. Geometrically, the spectrum has a negative convexity feature at frequency ν when its second derivative at ν is less than zero

($S''(\nu) < 0$). For the mean power spectral density of the ICs corresponding to rapid head movement, it is observed for the frequency range of 0.5–4.5 Hz that there is either a spectral peak or a negative convexity feature without a spectral peak. For the ICs corresponding to the cardioballistic (CB) motions, obvious spectral peaks are observed in 2–7 Hz part of the spectrum. To categorize the physical origin of an IC, the spectrum is divided into different frequency ranges (Figs. 2(a)–(f)): rapid head movement (RM: 0.5–4.5 Hz), cardioballistic motion (CB: 2–7 Hz), blink and saccade (BS: 0.5–3 Hz), and neuronal alpha activity (NR: 8–12 Hz). The BS and NR frequency ranges are examined so that possible blink and saccade ICs, as well as ICs corresponding to EEG alpha activity, can be identified and excluded from the motion IC candidates. The spectrum beyond 12 Hz is not considered in the analysis. Technical details of the automatic analysis of IC spectra are described in the Supplementary materials (Section S1, Tables S1–S3).

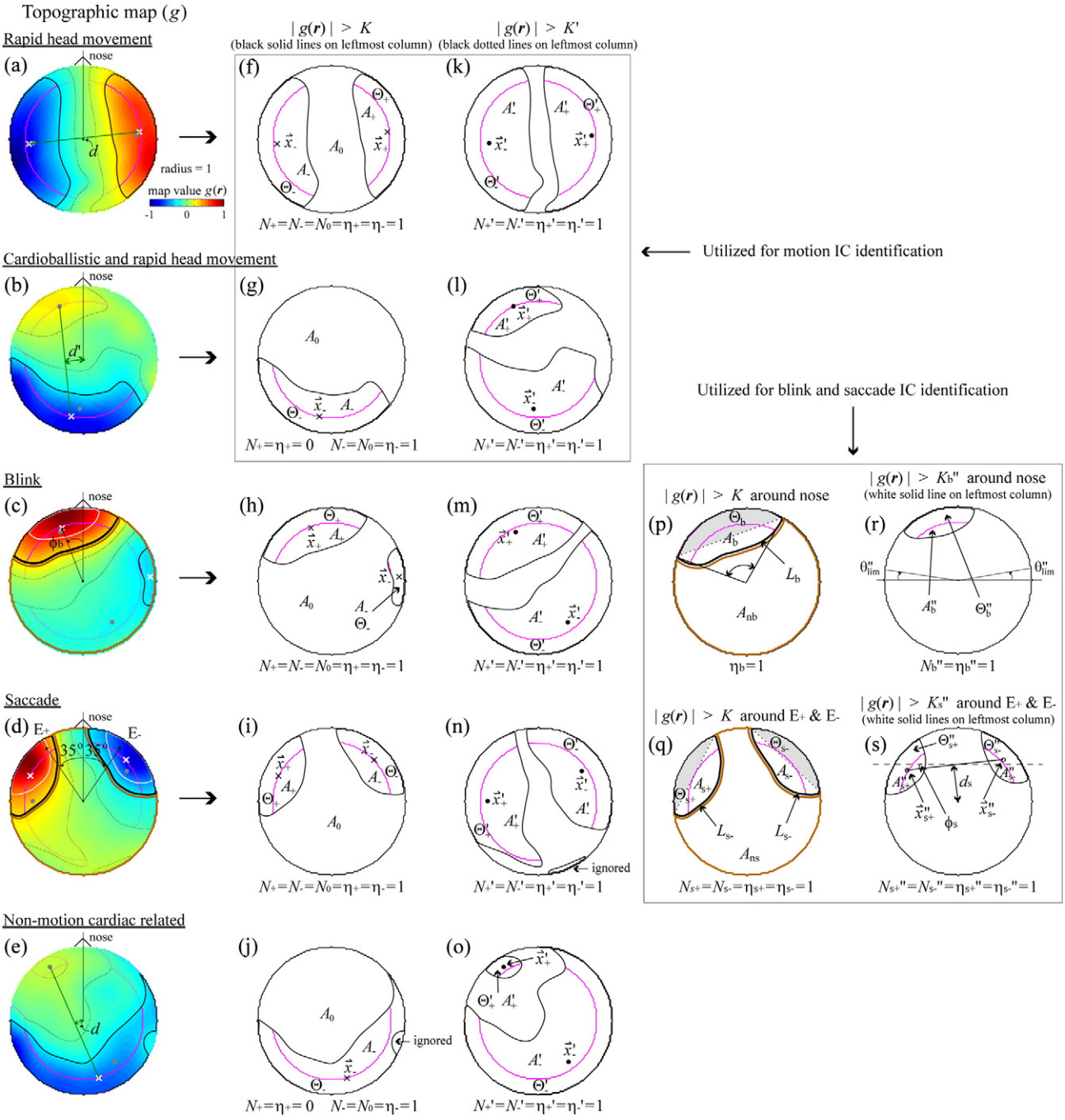

Fig. 3. The topographical maps for (a) the IC corresponding to rapid head movement in Fig. 2(a); (b) the IC mixture of rapid head movement and cardioballistic motion in Fig. 2(c); (c) the blink IC in Fig. 2(e); (d) the saccade IC in Fig. 2(f); (e) the example of a non-motion cardiac–related IC. The map boundary with width 0.2 is marked with magenta lines. In (a)–(e), the primary polarity regions ($|g(\boldsymbol{r})| > K$) are enclosed in black solid lines and the geometrical centers are marked with white crosses. The secondary polarity regions ($|g(\boldsymbol{r})| > K'$) are enclosed in black dotted lines and the centers are marked with gray dots. Here $(K, K') = (0.3, 0.1)$ are the threshold values. (f)–(j) plot the primary polarity regions of (a)–(e) explicitly with the geometrical centers marked as $\boldsymbol{x}_{\pm}$. (k)–(o) plot the secondary polarity regions of (a)–(e) explicitly with the geometrical centers marked as $\boldsymbol{x}_{\pm}'$. (p)–(q) show the primary polarity regions around the positions of the nose in (c) and $E_{\pm}$ in (d) respectively. The points $E_{\pm}$ are defined at a distance 0.9 from the origin and at an angle 35° from the vertical line joining the origin and the nose. (r)–(s) show the central regions enclosed in white solid lines around the positions of the nose in (c) and $E_{\pm}$ in (d). (f)–(g) and (k)–(l) are utilized in the identification of motion ICs. (p)–(s) are utilized in the blink and saccade ICs identification. In (r), the two angles $\theta_{\text{lim}}'' = 10°$ from the horizontal line are the extension limit of the central region in the topography of a blink IC. Other symbols are defined in Section S2.1.

Motion IC identification through topographic map analysis

The spatial projection of an IC contribution onto the EEG channel space forms the IC topographic map (Fig. 3(a)–(e)). The topographic map of an IC is computed by spatially interpolating the corresponding column of the ICA back-projection matrix $\{b_{ij}\}$ in Eq. (1) using the MATLAB function griddata(). When the head undergoes a simple rigid-body rotation in the uniform magnetic field of the MRI scanner, spurious conductive contours on the opposite sides of the EEG array typically experience magnetic flux changes of opposite signs, giving bilateral opposite polarities for EEG channels on the opposite sides of the EEG array (Zotev et al., 2012). In principle, the IC contributions for such opposite-side EEG channels should be of the same order of magnitude, so that the topographic map remains bipolar if a sufficiently high magnitude threshold is applied. In practice, bilateral opposite polarities with asymmetric magnitudes are often observed in an IC mixture of random and CB motions. Examples of topographic maps for motion ICs with symmetric and asymmetric magnitudes are shown in Figs. 3(a) and (b). It should be noted that not all cardiac-related ICs (McMenamin et al., 2010) can be used for E-REMCOR, but only those that are clearly cardioballistic in nature. For example, cardiac beats can be accompanied by deformations of the soft padding underneath the subject's head causing deformations of the EEG leads for the occipital EEG channels. The resulting artifacts have periodicity of the cardiac activity and unilateral topography, but their relation to the rigid-body head motion parameters is indirect and nonlinear. An example of the non-motion cardiac-related IC is shown in Fig. 3(e).

In aE-REMCOR, topographic maps of various ICs are analyzed automatically with certain requirements for IC polarity regions, including positions of the polarity regions, minimum region areas and arc region areas (Fig. 3(f)–(s)). Possible blink or saccade ICs are also identified by their topographic properties in addition to the motion IC candidates. Technical details of the automatic analysis of IC topographies are described in the Supplementary materials (Section S2, Tables S4–S5).

Motion IC identification through analysis of EEG signal contribution

Rapid and random head movements produce prominent spikes with durations of no less than tens of milliseconds in the EEG signal time courses, particularly for the electrodes near the edges of the EEG array. Similar spikes are evident in the time courses of the corresponding motion-related ICs. Removing the contributions of such motion-related ICs from the EEG data reduces the spikes significantly. Cardioballistic (CB) motions also produce signal spikes, which, however, are distributed more evenly across the EEG signal time course. Removal of the cardioballistic IC contributions leads to a steady signal reduction at the CB peak positions. EEG signals without the contribution of a particular IC, which we denote $V_i'(t)$, can be obtained using Eq. (1) with the corresponding column of the back-projection matrix $\{b_{ij}\}$ set to zero. The signal reduction after the removal of a selected IC is thus equal to the time course of that IC times the spatial projection constant for a given EEG channel.

In aE-REMCOR, the signal reduction at the i-th electrode ($|V_i(t)-V_i'(t)|$) after the removal of a particular IC is evaluated for the time periods corresponding to rapid head movements and/or cardiac beats. This approach is illustrated in Fig. 4. To identify a motion IC candidate, signal reduction criteria should be satisfied for a minimum number of EEG electrodes located close to the edges of the EEG array. Technical details of the automatic analysis of IC contributions are described in the Supplementary materials (Section S3, Tables S6-S8).

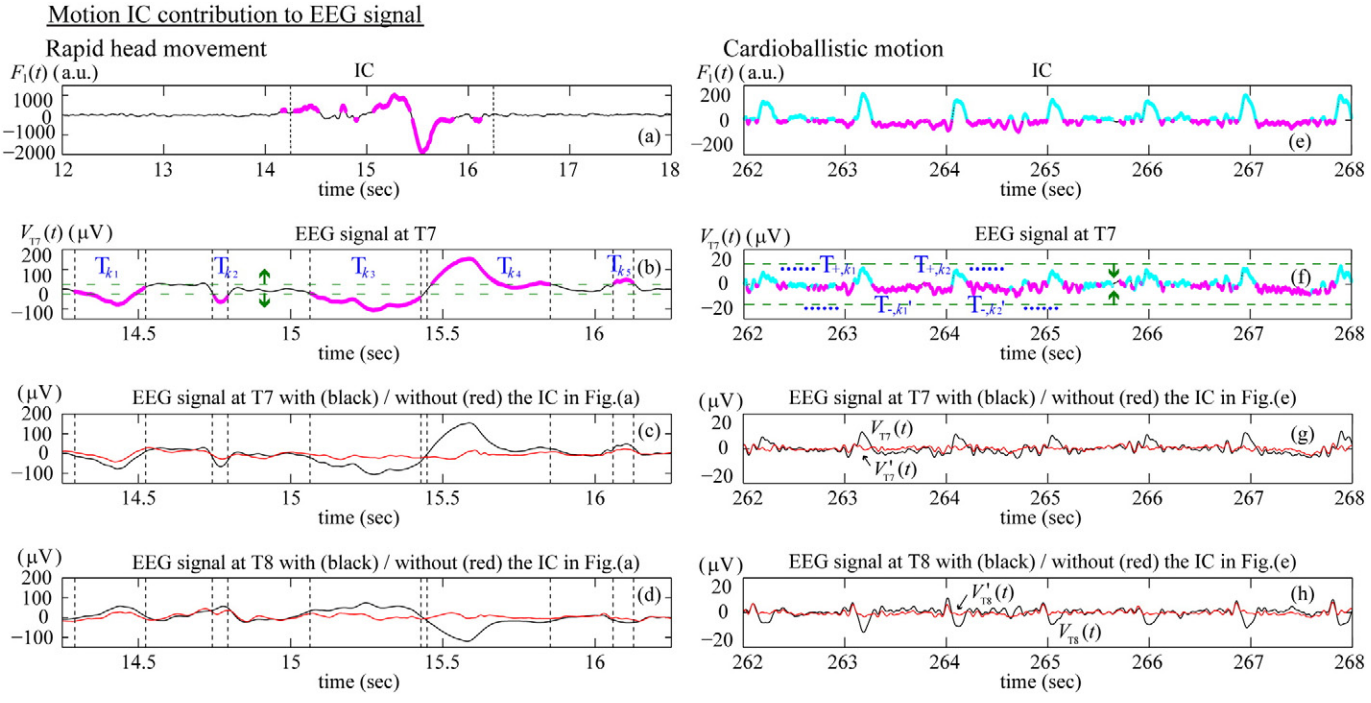

Fig. 4. (a) The time course of the rapid head movement IC, $F_1(t)$, shown previously in Figs. 2(a) and 3(a). (b) The time course of the signal measured at electrode T7 ($V_{T7}(t)$). (c)–(d) The time courses of the signal measured at electrode T7 and T8 before (black) and after (red) the removal of the IC in (a). (e) The time course of the cardioballistic motion IC shown in Figs. 2(b) and 7(c). (f) The time course of the signal measured at electrode T7 ($V_{T7}(t)$). (g)–(h) The time courses of the signal measured at electrode T7 and T8 before (black) and after (red) the removal of the IC in (e). The dotted lines in (a) indicate the time period in (b). In (a), the magenta line segments indicate the time periods when $F_1(t)$ is larger (smaller) than the threshold value $F_{1,0} + 4\sigma_{F1}$ ($F_{1,0}$-$4\sigma_{F1}$). In (b), the green dashed lines plot the threshold values $V_{T7,0} \pm 4\sigma_{T7}$. Each magenta line segment (T_k) in (b) represents the examination time period for the rapid head movement IC when the extremum of $V_{T7}(t)$ during the indicated period in (a) is greater than $V_{T7,0} + 4\sigma_{T7}$ or smaller than $V_{T7,0}$-$4\sigma_{T7}$. In (e), cyan and magenta line segments indicate the time periods when $F_1(t)$ is larger (smaller) than $F_{1,0} + 0.1\sigma_{F1}$ ($F_{1,0}$–$0.1\sigma_{F1}$). In (f), the green dashed lines plot the threshold values $V_{T7,0} \pm 4\sigma_{T7,min}(\tau = 10\ s)$. Here $F_{1,0}$, σ_{F1}, $V_{T7,0}$, σ_{VT7} and $\sigma_{T7,min}$ are defined in Eqs.(S4), (S5) and (S7). Each cyan (or magenta) line segment $T_{+,k}$ ($T_{-,k'}$) in (f) indicates the examination time period for the cardioballistic motion IC when the signal at T7 during the indicated period in (e) is bounded by the threshold values $V_{T7,0} \pm 4\sigma_{T7,min}(\tau = 10\ s)$.

Analysis of aE-REMCOR performance

A set of EEG based motion regressors are constructed by time integrating the selected motion ICs (Eq.(3)). These regressors are utilized to correct for head movements in the fMRI dataset on a slice-by-slice basis using AFNI 3dTfitter (Eq.(4)). The correction performance of aE-REMCOR on the fMRI dataset is examined using temporal signal-to-noise ratio (TSNR), motion parameters of the brain voxels, and improvement in the resting state fMRI (rs-fMRI) connectivity analysis. The maximum displacements of the voxels for each brain volume, the root mean square difference between an fMRI volume and the 1st volume, and the motion parameters (displacements dS, dL, dP in the superior–inferior, left–right and posterior–anterior directions, and rotation angles yaw, pitch and roll about the above directions) are estimated by AFNI 3dvolreg. For each scan, the above motion parameters with and without aE-REMCOR application are evaluated.

The temporal signal-to-noise ratio of an fMRI image is given by (Bodurka et al., 2007)

$$\mathrm{TSNR}(\boldsymbol{r}) = mean\left(S_{fMRI}(\boldsymbol{r},n), n=1,\ldots,N_{fMRI}\right)/\mathrm{std}\left(S_{fMRI}(\boldsymbol{r},n),\ \ n=1,\ldots,N_{fMRI}\right), \tag{5}$$

where $S_{\mathrm{fMRI}}(\boldsymbol{r},n)$ is the signal magnitude at the position $\boldsymbol{r}$ in the n^{th} brain volume of the fMRI dataset, and N_{fMRI} is the total number of the brain volume. The improvement of the TSNR($\boldsymbol{r}$) between the fMRI datasets with and without aE-REMCOR application (ΔTSNR($\boldsymbol{r}$)), and the average

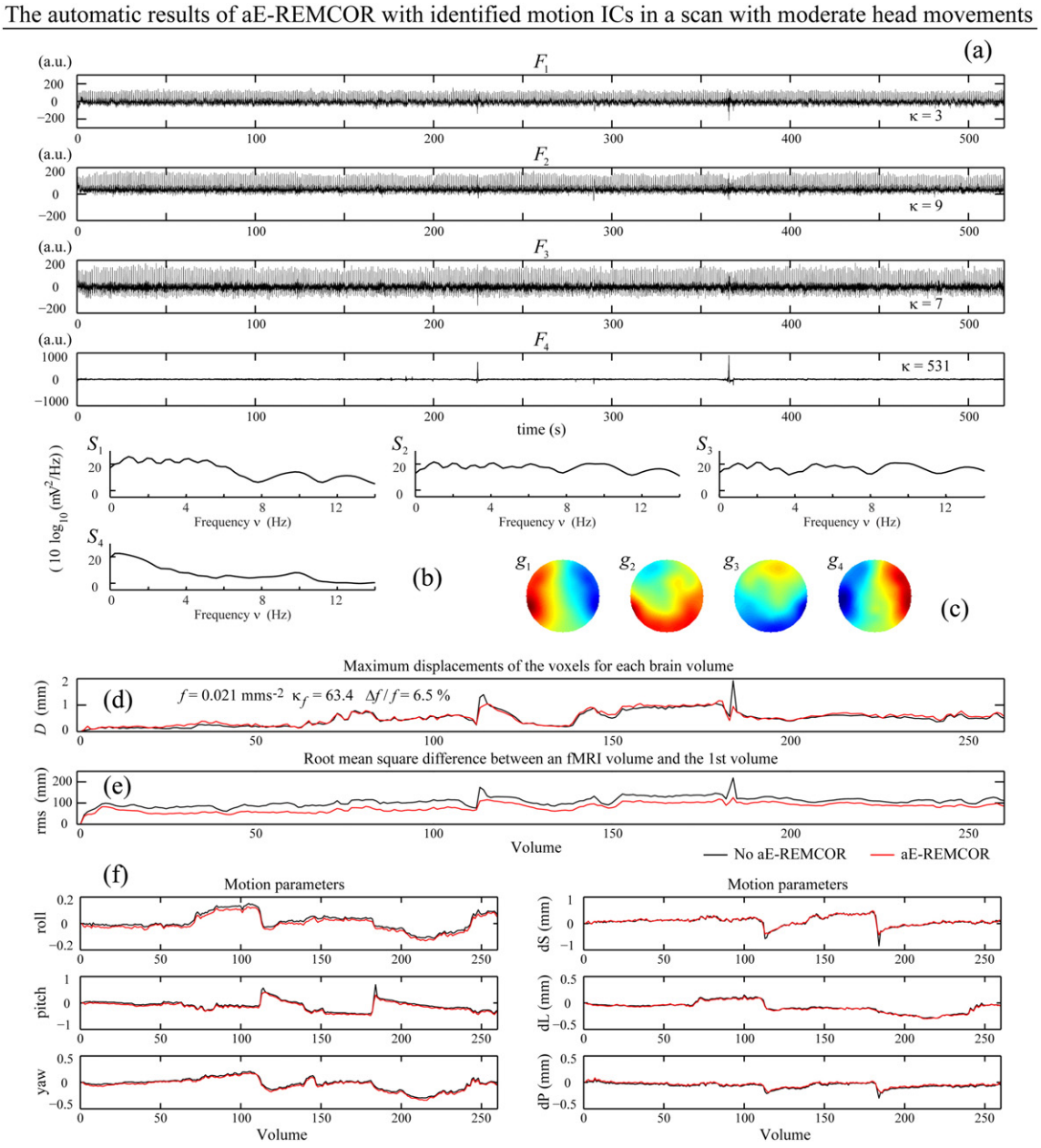

Fig. 5. The automatic results of aE-REMCOR with identified motion ICs in a scan with moderate rapid head movements. (a) The time courses, (b) spectra, (c) topographic maps of the identified motion IC. (d) The maximum displacement of the voxels (*D*) for each brain volume. (e) The root mean square difference (rms) between an fMRI volume and the 1st volume. (f) The rotation angles roll, pitch, yaw and the displacements along the superior (dS), left (dL) and posterior (dP) directions calculated by AFNI 3dvolreg. (g) The ΔTSNR plots on the slices of the brain along the axial direction without volume registration (upper plot) and with volume registration (lower plot). In (d)–(f), the results with and without aE-REMCOR are respectively plotted in red and black lines.

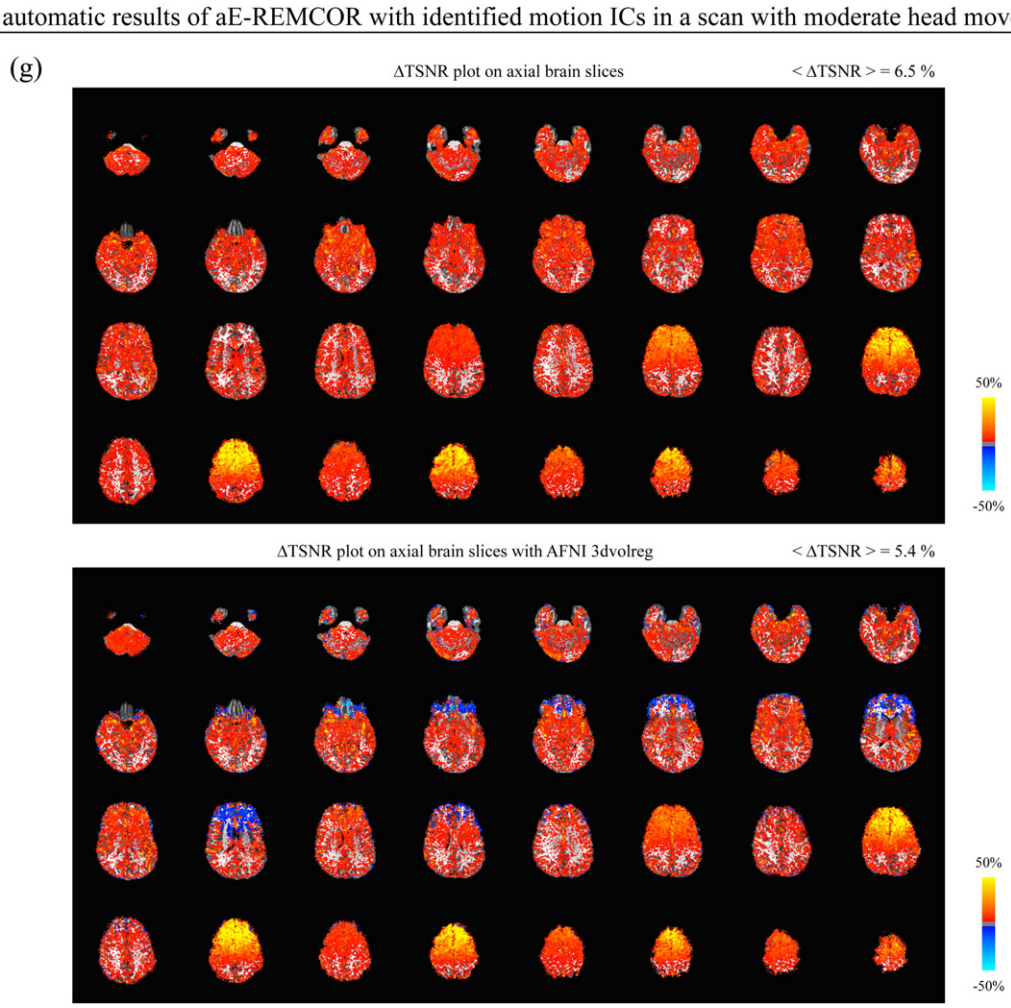

Fig. 5 (*continued*).

of ΔTSNR($\boldsymbol{r}$) over the brain.

$$\langle \Delta\text{TSNR} \rangle = mean(\Delta\text{TSNR}(\boldsymbol{r}), \boldsymbol{r} \in whole\ \ volume\ \ of\ \ the\ \ brain) \quad (6)$$

are examined for each scan. To understand the combined effects of aE-REMCOR and the standard fMRI preprocessing procedure, ΔTSNR and ⟨ΔTSNR⟩ are also evaluated with the volume registration using AFNI 3dvolreg applied to both the original and aE-REMCOR corrected datasets.

In the rs-fMRI connectivity analysis, we compared the seed-based (posterior cingulate cortex) default-mode network (DMN) connectivity results performed with and without aE-REMCOR. When aE-REMCOR was applied, it was employed before the fMRI preprocessing steps: slice-timing correction, volume registration, and Talairach coordinate registration (Talairach and Tournoux, 1998). Then the fMRI data was spatially blurred to 4-mm FWHM and temporally bandpass filtered at 0.01–0.08 Hz to reduce the effect of low-frequency drift and high-frequency noise (Biswal et al., 1995; Lowe et al., 1998). The rs-fMRI connectivity of the DMN was examined in 86 resting scans using GLM-based correlation analysis (Friston, 2005; Van Dijk et al., 2010). A spherical seed ROI with radius 5 mm was centered at the posterior cingulate cortex (PCC) (Talairach coordinate: (0, −51, 22) (Van Dijk et al., 2010)). Nuisance covariates included cerebrospinal fluid signal, white matter signal, and the 6 rigid body motion parameters (dS, dL, dP, yaw, pitch and roll). We evaluated the correlation and the correlation difference of the data with and without aE-REMCOR. We also quantified the correlation changes in medial prefrontal cortex (mPFC: (0, 49, 2)), lateral parietal cortex (LatPar-L: (−45, −60, 32), LatPar-R: (43, −60, 29)), and hippocampal formation (HF-L: (−22, −19, −15), HF-R: (22, −19, −15)) of the DMN (Van Dijk et al., 2010).

Results

Automatic identified motion ICs

Figs. 5-7 show the automatic results of aE_REMCOR with identified motion ICs from scans with examples of moderate, significant and little rapid head movements respectively. In each figure, the time courses, spectra, and topographic maps of the selected motion IC, as well as the motion information acquired with AFNI 3dvolreg and the TSNR improvement, are plotted. For the scan shown in Fig. 5, four motion ICs are identified. The first three ICs are identified as cardioballistic motion ICs and the fourth is identified as the rapid head movement IC (Supplementary Table S9). In this scan, the two kinds of motions are well separated in the selected motion ICs with little mixing of the other components. However, such a well separation of components is not always the case with the ICA, especially when there are significant motions during the scan.

Fig. 6 shows the results from a scan with significant subject motions. For this scan, five motion ICs are identified. The 1st, 2nd, 4th and 5th IC ($F_1(t)$, $F_2(t)$, $F_4(t)$, $F_5(t)$) are identified as the rapid head movement ICs, and the 3rd IC ($F_3(t)$) is identified as the cardioballistic motion IC. The spectra, and topographic maps of the 1st and 3rd ICs are shown previously in Figs. 2(a), 3(a) and 2(c), 3(b). The time course of the 1st IC is

shown in Fig. 4(a). In the time course of $F_3(t)$, in addition to the obvious spikes caused by the rapid head movements, distinct cardiac pulses are also observed (Fig. 6(h)). Indeed $F_3(t)$ is a significant mixture of cardioballistic motion and rapid head movement components due to the incomplete separation of the ICA. Thus a more accurate interpretation about the identification algorithm on the random head and cardioballistic motions in Suplementary Table S9 is that the algorithm actually estimates the dominant component of the IC, instead of distinguishing each IC with only one physical origin.

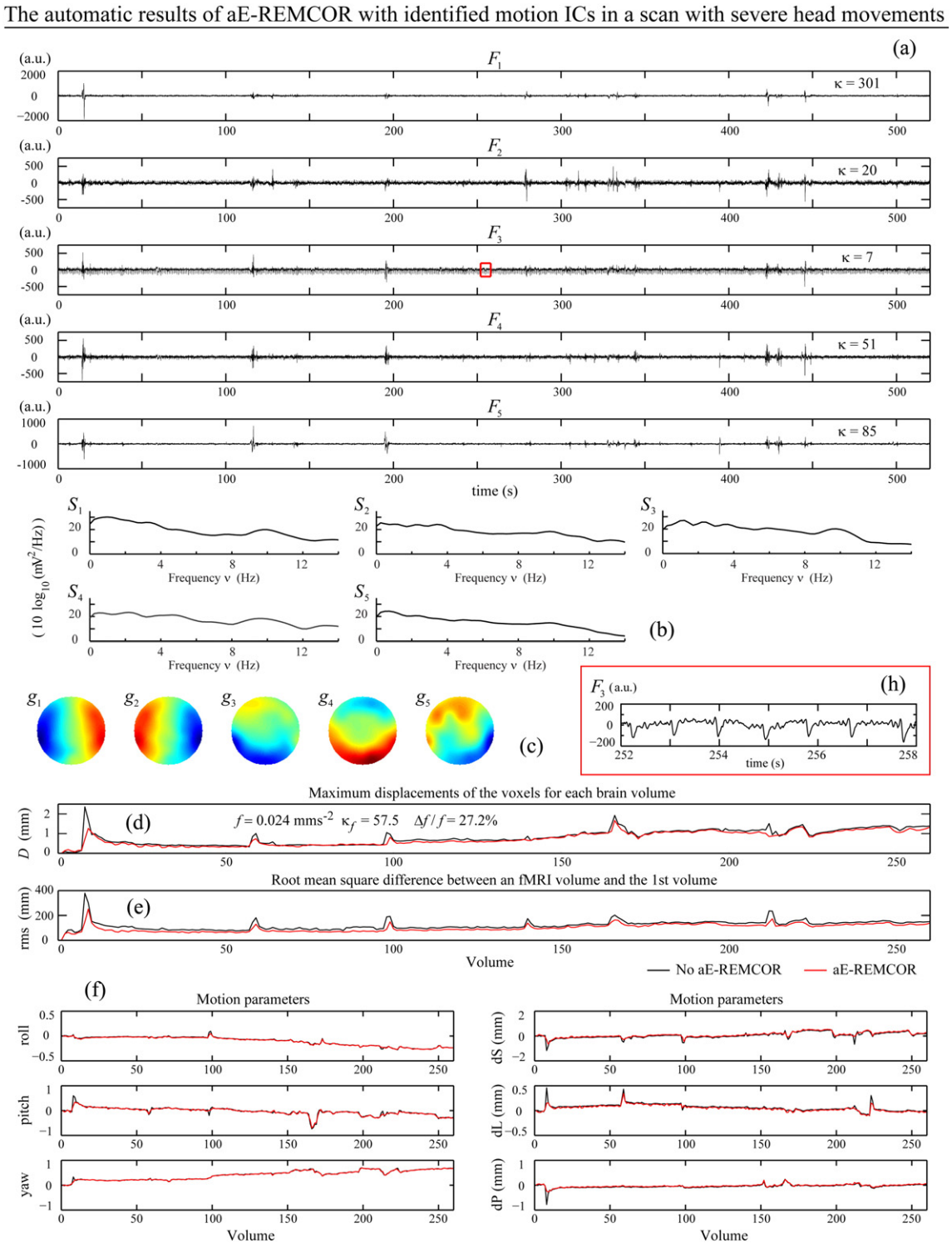

Fig. 6. The automatic results of aE-REMCOR with identified motion ICs in a scan with severe rapid head movements. (a) The time courses, (b) spectra, (c) topographic maps of the identified motion IC. (d) The maximum displacement of the voxels (D) for each brain volume. (e) The root mean square difference (rms) between an fMRI volume and the 1st volume. (f) The rotation angles roll, pitch, yaw and the displacements along the superior (dS), left (dL) and posterior (dP) directions calculated by AFNI 3dvolreg. (g) The ΔTSNR plots on the slices of the brain along the axial direction without volume registration (upper plot) and with volume registration (lower plot). (h) The close-up of the red box in (a). In (d)–(f), the results with and without aE-REMCOR are respectively plotted in red and black lines.

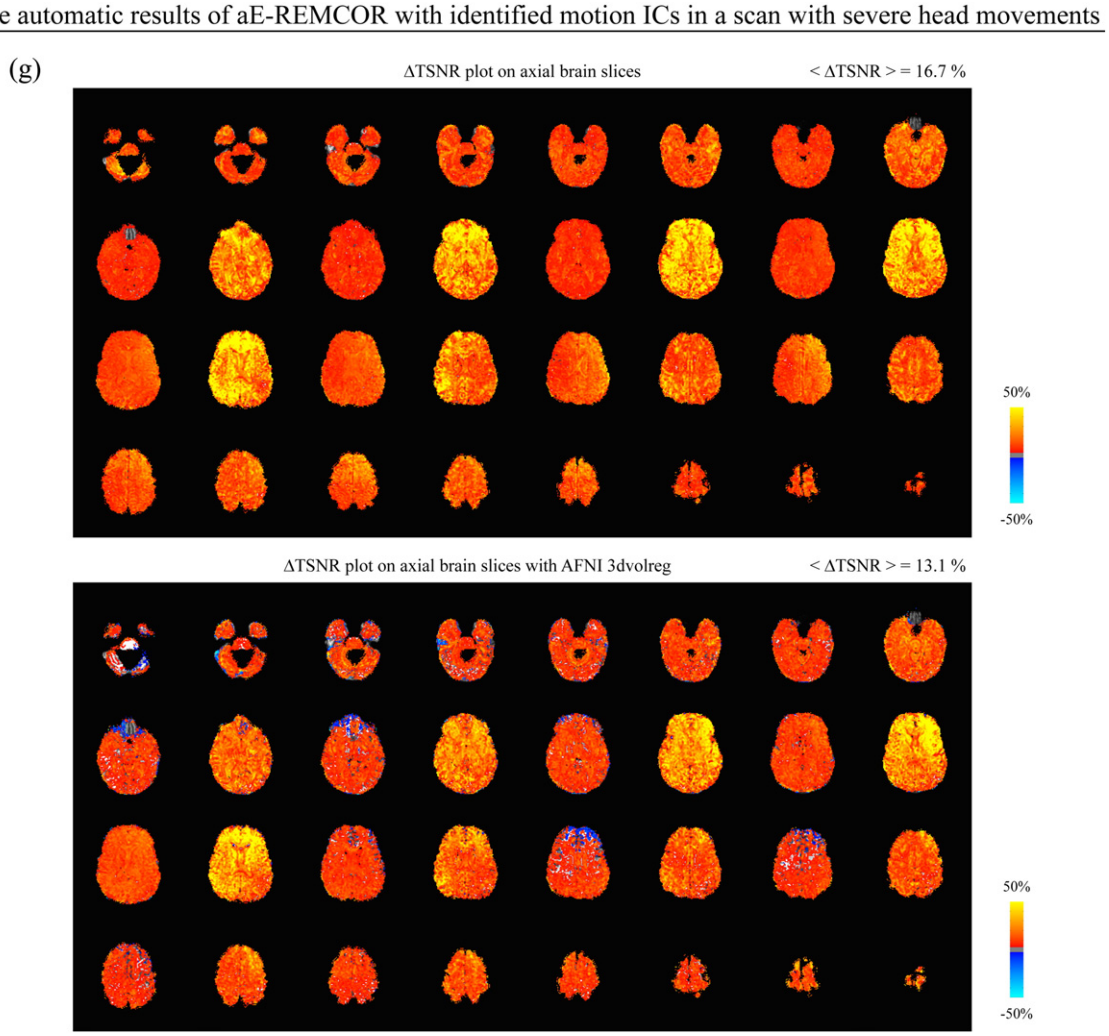

Fig. 6 (*continued*).

TSNR improvement

The ΔTSNR with and without the volume registration using AFNI 3dvolreg are plotted on the slices of the brain along the axial direction in Figs. 5(g) and 6(g). The figures show that larger ΔTSNR are obtained on the brain edge regions, as these areas are affected the most by the rapid head movement. Also, the motion correction in a particular time period gives similar ΔTSNR pattern in alternative slices, since with the SENSE acceleration factor = 2 used for the fMRI image acquisition, the first half of the interleaved images are acquired in one time period, and the remaining half of the interleaved images are acquired in the other time period. In Figs. 5(g) and 6(g), the average improvements of the TSNR over the brain (⟨ΔTSNR⟩) without volume registration are 6.5% and 16.7% (5.4% and 13.1% with volume registration). The corresponding top 10^{th} percentile of ΔTSNR without volume registration reaches over 14.3% and 33.9% (14.6% and 28.2% with volume registration).

Fig. 7 shows the results from a scan with little subject motion. For this scan, one IC is identified as the cardioballistic motion IC. No significant improvement is observed in TSNR (Fig. 7(g)), and ⟨ΔTSNR⟩ without volume registration is increased by 1.1% (1.4% with volume registration). While aE-REMCOR is shown to be capable of substantially removing head movements in the fMRI dataset in Figs. 5 and 6, it does not necessarily improve much the image quality for the scan with little head movements as the motion artifact in the fMRI data is small. Since a larger ⟨ΔTSNR⟩ can be obtained in the scans with more severe motions, it is thus expected that the efficiency of aE-REMCOR depends on the motion severity.

Figs. 5(d)–(f), 6(d)–(f) and 7(d)–(f) show the maximum displacement of the voxels for each brain volume (D), the root mean square difference between an fMRI volume and the 1^{st} volume (rms), and the motion parameters (roll, pitch, yaw, dS, dL, dP) calculated by AFNI 3dvolreg. The spikes in D, rms and the motion parameters indicate the occurrences of the rapid head movements. With the application of aE-REMCOR, the spikes in Figs. 5(d)–(f) and 6(d)–(f) are significantly reduced, and the fluctuations in Fig. 7 (d)–(f) are also slightly smoothed.

Efficiency of aE-REMCOR

The rapid change in the magnitude of the maximum displacements of the voxels for each brain volume (Figs. 5(d), 6(d) and 7(d)) can be used to characterize the severity of the head movements for the examination of the efficiency of aE-REMCOR. To measure the fluctuations of the maximum displacement for the brain voxels (D), the second derivative $d^2D(n)/dn^2$ is calculated, where n is the number index of the brain volume. The head movement severity is defined by the average magnitude of the second derivative over the entire scan, and is given by

$$f = mean\left(\left| d^2D(n)/dn^2 \right| \Big/ (\Delta t)^2, n = 1, \ldots, N_{fMRI}\right). \quad (7)$$

Here $\Delta t = 2$ s is the time interval between the acquisitions of two consecutive brain volumes, which is equal to the repetition time of the fMRI scan. The motion severities with and without the application of

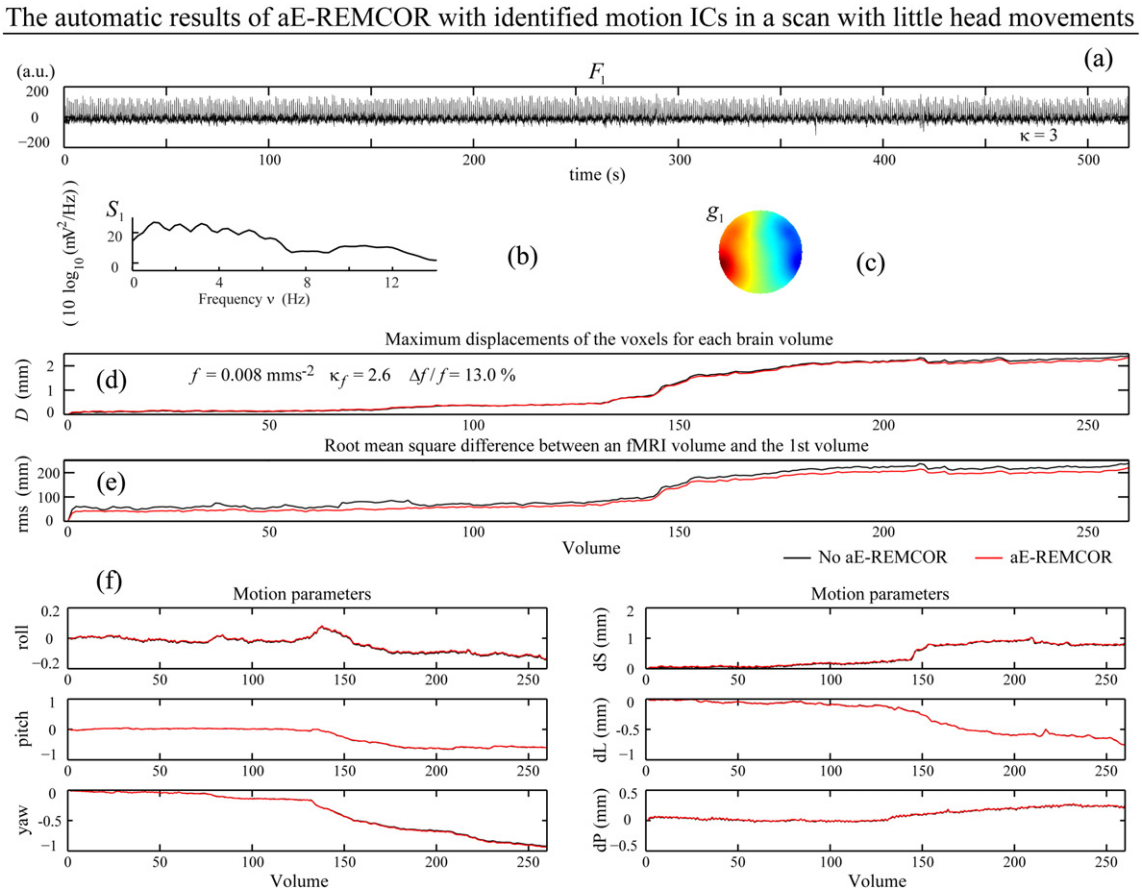

Fig. 7. The automatic results of aE-REMCOR with identified motion ICs in a scan with little head movements. (a) The time courses, (b) spectra, (c) topographic maps of the identified motion IC. (d) The maximum displacement of the voxels (D) for each brain volume. (e) The root mean square difference (rms) between an fMRI volume and the 1st volume. (f) The rotation angles roll, pitch, yaw and the displacements along the superior (dS), left (dL) and posterior (dP) directions calculated by AFNI 3dvolreg. (g) The ΔTSNR plots on the slices of the brain along the axial direction without volume registration (upper plot) and with volume registration (lower plot). In (d)–(f), the results with and without aE-REMCOR are respectively plotted in red and black lines.

aE-REMCOR are denoted by f' and f respectively. Note that the motion severity f signifies the fast changing spiky features of D instead of the slowly varying components. It can be interpreted as the average acceleration of the head motions during the scan. Thus a larger f usually indicates occasional or prolonged period of rapid head movements during the scan. To distinguish these two situations, the kurtosis of $d^2D(n)/dn^2$ is calculated:

$$\kappa_f = \text{kurtosis}\left(d^2D(n)/dn^2/(\Delta t)^2, n = 1, \ldots, N_{\text{fMRI}}\right). \quad (8)$$

Kurtosis is a measure of non-Gaussianity. For prolonged period of rapid head movements, the distribution of $d^2D(n)/dn^2$ tends to become more Gaussian by the Central Limit Theorem, giving a small κ_f and a large f. The occasional rapid head movements, on the other hand, will give rise to a large κ_f and a moderate f. Finally, a small κ_f and a small f indicate the absence of significant head motions.

The aE-REMCOR was applied to 305 fMRI scans. The average improvement ⟨ΔTSNR⟩ is plotted against f in Fig. 8(a), (c), and the improvements ΔTSNR($\boldsymbol{r}$) at the upper (blue dots) and lower (red dots) 10th percentile are plotted in Fig. 8(b), (d). It should be noted that a larger ⟨ΔTSNR⟩ can usually be achieved in the scans with large f and κ_f. In other words, a higher aE-REMCOR efficiency can be obtained when there are severe head movements during the scan. With aE-REMCOR, the largest average improvement over the brain ⟨ΔTSNR⟩ goes up to 27%, and the corresponding top 10% of the ΔTSNR reaches over 55%. The average ⟨ΔTSNR⟩ over the scans with prolonged ($f > 0.10$) and occasional ($\kappa_f > 40$) rapid head movements in Fig. 8(a) are 13.7% and 7.7% (9.1% and 5.2% in Fig. 8(c)). This shows a higher correction performance in scans with prolonged rapid head movements than in scans with occasional rapid head movements. In most cases when the subjects have no significant motion (small f and κ_f), ⟨ΔTSNR⟩ increases slightly by a few percent, indicating the effectiveness of aE-REMCOR in removing the cardioballistic motions in the fMRI dataset.

The decrease in the motion severity $\Delta f = f - f'$, which quantifies the smoothing of the fluctuations in D after motion correction, is another measure of the efficiency of the aE-REMCOR. For instance, if aE-REMCOR removes all traces of motions, the maximum displacement of the voxels for all brain volumes ($D(n)$, $n = 1, \ldots, N_{\text{fMRI}}$), and hence f', vanishes. In this limit, $\Delta f/f = 1$. In the other extreme, if the EEG based regressors fail to carry any motion information, f' can be any number larger than f depending on the performance of AFNI 3dTfitter. In this case, $\Delta f/f \le 0$. In reality, there is an upper limit for the efficiency ratio $\Delta f/f$. The ratio is smaller than one as D is unlikely to be zero after the motion correction because of the noise and inaccurate representation of motions in the EEG data and also the fMRI data. Fig. 9(a) plots Δf against f for the 305 scans, and Fig. 9(b) plots the efficiency ratio $\Delta f/f$. Similar to the TSNR analysis, a higher efficiency ratio $\Delta f/f$ can usually be achieved when there are severe head movements during the scan (large f). The maximum efficiency of the current aE-REMCOR algorithm can be approximated by the bounding slope of the plot, which is about 74%. The average efficiency over the 305 scans is 18%, and the maximum efficiency over the scans is 71%. aE-REMCOR is shown to be capable of improving the TSNR and reducing the motion severity in scans with rapid head movements and cardioballistic motions. Nevertheless one should be cautious in using 3dTfitter for cardioballistic motion correction in

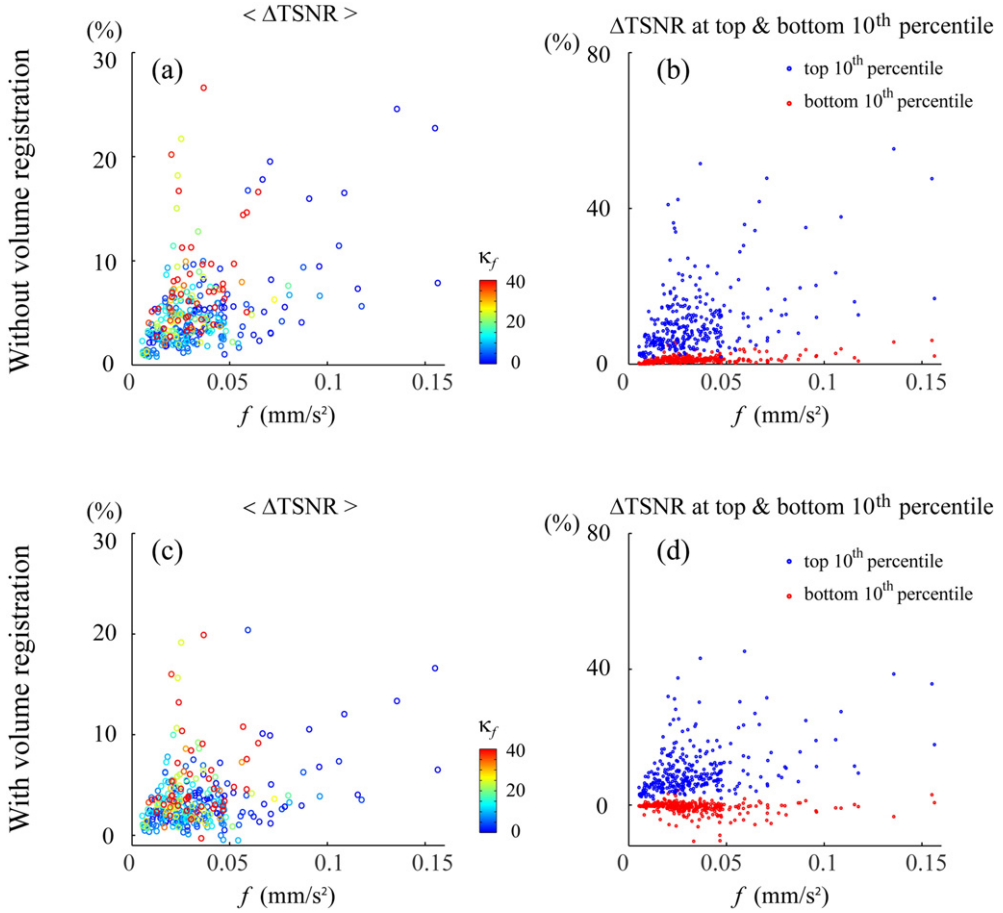

Fig. 8. The plots of (a), (c) the average improvement ⟨ΔTSNR⟩ against the motion severity *f*; (b), (d) the ΔTSNR at the upper (blue dots) and lower (red dots) 10th percentile against *f*. The ΔTSNR in (a)–(b) are calculated without volume registration. The ΔTSNR in (c)–(d) are calculated with volume registration (AFNI 3dvolreg). The color used in (a) and (c) is scaled to the kurtosis of the second derivative of the maximum displacement *D* defined in Eq. (8).

experiments with small signal-to-noise ratio, as any inefficient motion correction will introduce relatively significant overcorrection in the fMRI images.

rs-fMRI connectivity analysis.

The utility of aE-REMCOR to improve the rs-fMRI connectivity of the default mode network (DMN) is examined with the seed-based correlation analysis in this section. The motion severity parameters *f* and κ_f for the resting scans are summarized in Fig. 10. These parameters are used to choose the scanning group with occasional rapid head movements ($\kappa_f > 40$: the 7 scans in red circle) and the scanning group with prolonged period of rapid head movements ($f > 0.10$: the 4 scans in blue circle).

Fig. 11(a)–(b) plot the rs-fMRI DMN correlation maps for the scan previously shown in Fig. 6. Stripes are observed in Fig. 11(a) for the correlation map without aE-REMCOR. The stripes can be seen clearly in the correlation difference (Fig. 11(c)). This stripe pattern originates

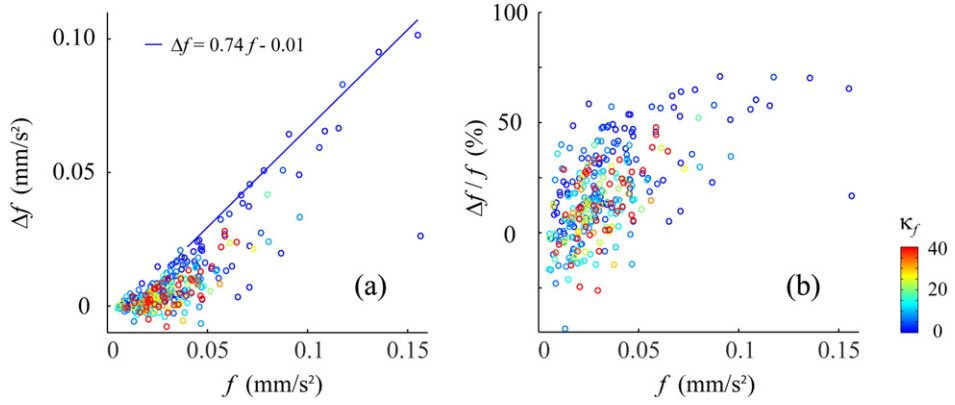

Fig. 9. The plots of (a) Δ*f* against the motion severity *f*; (b) the efficiency ratio Δ*f*/*f* against *f*. The color used in (a) and (b) is scaled to the kurtosis of the second derivative of the maximum displacement *D* defined in Eq.(8).

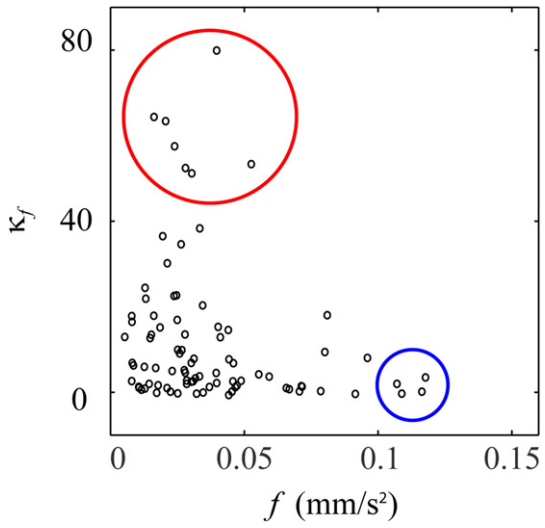

Fig. 10. The summary of the motion severity parameters f and κ_f in resting scans. The scans with $\kappa_f \geq 40$ and $f \geq 0.1$ to be used in the rs-fMRI connectivity analysis in Figs. 11(d)–(f) are enclosed in red and blue lines.

from the motion-induced signal loss in neighboring imaging slices as discussed in Section 3.2. When aE-REMCOR is applied, the contrast of the stripes reduces (Fig. 11(b)). Fig. 11(d)–(f) plot the group correlation differences in scans with occasional ($\kappa_f > 40$), prolonged ($f > 0.10$), and both kinds of rapid head movements ($\kappa_f > 40$ or $f > 0.10$). Similar motion-induced stripes with a lower contrast can be observed. The group correlation maps of the DMN for all resting scans are plotted in Fig. 11(g) and (h). The corresponding group correlation difference ((h) - (g)) is shown in Fig. 11(i). When all the 86 resting scans are considered, the motion-induced stripes disappear (Fig. 11(i)). This shows the reduced significance of motion artifacts on the DMN connectivity when sufficient scans with little head motion are considered. Nevertheless, when the entire group of subjects exhibits significant rapid head movements, slice-by-slice fMRI motion correction is particular important to improve the accuracy of the rs-fMRI connectivity analysis. The centers of the ROIs in posterior cingulate cortex (PCC), medial prefrontal cortex (mPFC), lateral parietal cortex (LatPar-L, LatPar-R) and hippocampal formation (HF-L, HF-R) of the DMN are marked with crosshairs in Fig. 11. The correlation difference at a given ROI is denoted by ΔC(ROI's name). The correlation difference, its percentage change relative to the original correlation value without aE-REMCOR, and the p-value are calculated for different scanning groups. For all scanning groups, a slight correlation decrease is observed at the seed ROI: for $\kappa_f > 40$, $\Delta C(\text{PCC}) = -0.017$ (-2.2%, $p = 0.004$); for $f > 0.10$, $\Delta C(\text{PCC}) = -0.004$ (-0.7%, $p = 0.213$); for $\kappa_f > 40$ or $f > 0.10$, $\Delta C(\text{PCC}) = -0.012$ (-1.7%, $p = 0.003$); for all resting scans, $\Delta C(\text{PCC}) = -0.003$ (-0.4%, $p = 0.018$). For the group with $\kappa_f > 40$, a large correlation change is found at the hippocampal formation $\Delta C(\text{HF-R}) = 0.019$ (60.4%, $p = 0.018$). When all the resting scans are considered, $\Delta C(\text{mPFC}) = 0.002$ (1.1%, $p = 0.451$), $\Delta C(\text{LatPar-L}) = -0.007$ (-3.3%, $p = 0.018$), $\Delta C(\text{LatPar-R}) = -0.004$ (-2.1%, $p = 0.174$), $\Delta C(\text{HF-L}) = 0.006$ (8.8%, $p = 0.027$), and $\Delta C(\text{HF-R}) = 0.008$ (12.6%, $p = 0.005$). The changes are statistically significant in PCC, LatPar-L, HF-L, and HF-R.

Discussions

In this paper, automatic categorization algorithms were developed to provide quantitative descriptions and analyses on the features observed in the mean power spectral density, topographic map and signal contribution of an identified IC in the EEG data acquired simultaneously with fMRI. The algorithm aims to mimic the manual selection of the ICs related to head movements by adequately choosing the features that are commonly observed in the motion ICs. The effectiveness of the algorithm can be measured by its accuracy of reproducing the manual selection. From the examination of a total of 9455 ICs in 305 scans, there were 1045 true identification of motion ICs (TP), 8370 true identification of non-motion ICs (TN), 9 false identification of motion ICs (FP), and 31 false identification of non-motion ICs (FN), giving a precision $P_{\text{IC}} = \text{TP}/(\text{TP} + \text{FP}) = 99.15\%$, recall $R_{\text{IC}} = \text{TP}/(\text{TP} + \text{FN}) = 97.12\%$, and F-score $= 2P_{\text{IC}}R_{\text{IC}}/(P_{\text{IC}} + R_{\text{IC}}) = 98.12\%$.

The present categorization algorithm is utilized to select the motion ICs for the purpose of correcting head motions on slice-by-slice basis in the fMRI dataset. While the selected cardioballistic motion ICs manifest distinct cardiac pulses in each cycle, they are insensitive to the improper positioning of electrocardiogram (ECG) and are less sensitive to head motions when compared to the ECG. Thus there is an advantage in utilizing the selected cardioballistic motion ICs for applications like cardiac period and arrhythmia detections.

The developed automatic algorithm can also be utilized to preprocess the EEG data when it is applied in a reverse manner to remove, instead of to select, the identified rapid head movement ICs, cardioballistic motion ICs, and possible blink and saccade ICs from the EEG data. For the current purpose of motion ICs selection, a cardioballistic IC with exceedingly large power at high harmonic frequencies in the mean power spectral density or insignificantly small EEG signal contribution is not considered. For the purpose of preprocessing the EEG data, ICs related to cardioballistic artifact with large power at high harmonic frequencies and small signal contribution should also be selected for removal. With the preprocessed EEG data, further identification, such as for the alpha rhythm of the neuronal signal, is possible when the features of the mean power spectral density, topographic map and signal contribution are adequately chosen and the parameters are properly adjusted.

Currently parameters are determined empirically based on the commonly observed features in 305 scans from 16 subjects in a 3 T MRI scanner. The parameters may need to be adjusted when other than 3 Tesla MRI field strengths are used or more datasets are available. Given a huge amount of data, the identifications of motions will benefit from more systematic approaches, like logistic regression or support vector machine modeling. Nevertheless, the current automatic algorithm provides basic tools to understand the properties of the motion related ICs, the potential and limitation of the ICA, and the efficiency of the motion correction in the fMRI datasets with the EEG based regressors.

The calculations are carried out in a workstation with dual Intel® Xeon® CPU E5-2620 at 2.00GHz and 16GB memory. No explicit parallelization was implemented in the MATLAB code. The computation time of the ICA increases with the requested number of ICs, and the computation time of the motion correction procedures in AFNI increases with the number of selected motion ICs and the size of the image. Consider an fMRI dataset with 260 brain volumes, 34 axial slices per volume and an image matrix 128×128, and an EEG dataset with 31 ICs and 5 identified as motion ICs, the computation times (and percentage) of the main motion correction procedures are 13.9 s (2.3%) for the EEG data preprocessing, 137.5 s (22.4%) for the ICA, 8.6 s (1.4%) for the spectrum analysis, 3.9 s (0.6%) for the topography analysis, 31.9 s (5.2%) for the signal contribution analysis, 228 s (37.1%) for the AFNI regressors calculations in BRIK format, and 191.4 s (31.1%) for the AFNI 3dtfitter calculations. It should be noted that the computation times of the ICA and AFNI dominate the whole process. Thus their speeds critically determine the possibility of the aE-REMCOR in real-time application. Since the three motion IC identification analyses can be performed independently and simultaneously for each IC, the computation speed can be improved by parallelizing the algorithm. For the motion correction of the fMRI data in AFNI, the calculations, in principle, can also be sped up by parallelizing the algorithm with the use of graphic processing unit (GPU) (Misaki et al., 2015).

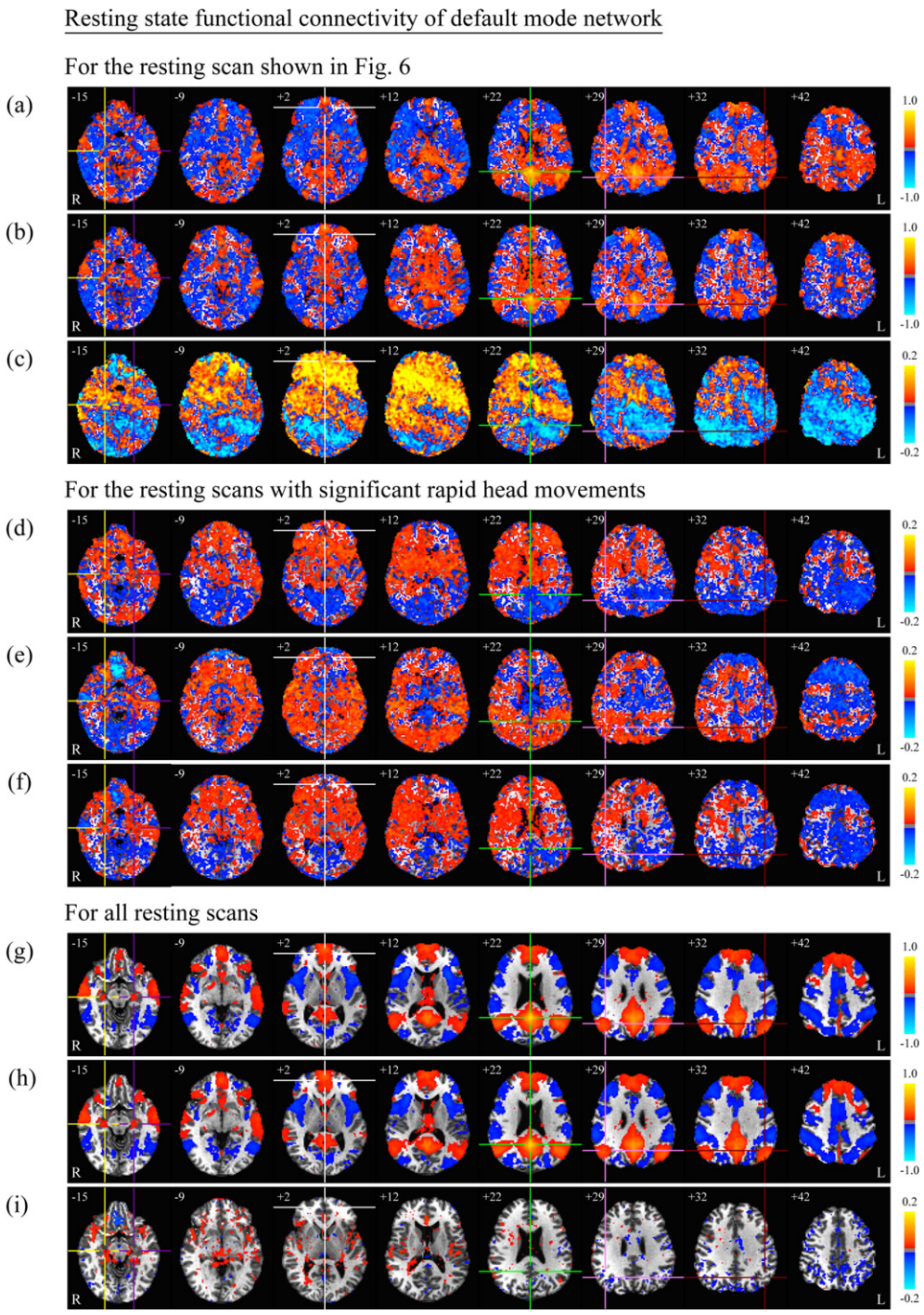

Fig. 11. Resting state connectivity of the default mode network (DMN). (a)–(b): Correlation map without and with aE-REMCOR for the scan with significant rapid head movements shown in Fig. 6. (c): Correlation difference ((b)–(a)). (d)–(f): Group correlation difference for the scans with occasional rapid head movements ($\kappa_f \geq 40$), prolonged rapid head movements ($f \geq 0.1$), and both ($\kappa_f \geq 40$ or $f \geq 0.1$). (g)–(h): Group correlation map without and with aE-REMCOR for all the 86 resting scans. (i): Group correlation difference for all the resting scans ((h)–(g)). The centers of the ROI in PCC (0, −52, 22), mPFC (0, 49, 2), LatPar-L (−45, −60, 32), LatPar-R (43, −60, 29), HF-L, (−22, −19, −15) and HF-R (22, −19, −15) of the DMN are respectively marked with green, white, maroon, pink, purple and yellow crosshairs. Indicated next to each slice image is the z-coordinate of the slice. For the group analysis in (g)–(i), uncorrected $p < 0.05$ is used.

Conclusions

An automatic EEG-assisted retrospective motion correction (aE-REMCOR) method that utilizes EEG data to correct for head movements in fMRI on a slice-by-slice basis is reported. The aE-REMCOR automatically preprocesses and analyzes the EEG data, identifies the independent components (ICs) corresponding to head motions, and constructs the EEG based regressors with the identified motion ICs. The entire automatic procedure is carried out in MATLAB. The motion artifacts in the fMRI images are corrected with the motion regressors in AFNI.

The automatic identification of the motion ICs is achieved by recognizing the special features of the motion artifacts imposed on the mean power spectral density, topographic map, and EEG signal contribution of the ICs. An automatic algorithm for the motion IC identification is developed. The algorithm is shown to be capable of identifying the ICs related to rapid head movements and cardioballistic motions, and also

the dominant component in the mixture of them when the ICA fails to separate the different motion components completely.

The aE-REMCOR is applied to 305 fMRI scans from 16 subjects in a 3 T MRI scanner. The results show that aE-REMCOR is capable of substantially removing head motions in fMRI images. With aE-REMCOR, the spikes and fluctuations of the motion parameters induced by the head movements are significantly reduced and smoothed. In particular, when there are significant rapid head movements during the scan, a large temporal signal-to-noise ratio (TSNR) improvement and high correction efficiency can be achieved. Depending on the subject's motion, the average TSNR improvement over the brain with aE-REMCOR goes up to 27% with the largest 10% of the TSNR improvement reaches over 55%. In the efficiency analysis for the motion correction, the average correction efficiency over the 305 scans is 18% and the largest achieved efficiency is 71%. It is observed from the results that the highest possible motion correction efficiency with the current aE-REMCOR algorithm is bounded by approximately 74%. The utility of aE-REMCOR on the fMRI connectivity of the default mode network (DMN) is examined in 86 resting scans. The motion-induced position-dependent error in the DMN connectivity analysis is shown to be reduced when aE-REMCOR is utilized. The results also show the importance of slice-by-slice fMRI motion corrections to improve the accuracy of rs-fMRI connectivity analysis when the entire group of subjects exhibits significant rapid head motions. The achieved automation procedure warrants its use in large clinical EEG and fMRI studies, and provides incentive for conducting simultaneous EEG & fMRI.

Acknowledgments

This work was supported by the U.S. Department of Defense grant W81XWH-12-1-0607.

Appendix A. Supplementary data

Supplementary data to this article can be found online at http://dx.doi.org/10.1016/j.neuroimage.2016.01.042.

References

Allen, P.J., Polizzi, G., Krakow, K., Fish, D.R., Lemieux, L., 1998. Identification of EEG events in the MR scanner: the problem of pulse artifact and a method for its subtraction. NeuroImage 8, 229–239.

Allen, P.J., Josephs, O., Turner, R., 2000. A method for removing imaging artifact from continuous EEG recorded during functional MRI. NeuroImage 12, 230–239.

Beall, E.B., Lowe, M.J., 2014. SimPACE: generating simulated motion corrupted BOLD data with synthetic-navigated acquisition for the development and evaluation of SLOMOCO: a new, highly effective slicewise motion correction. NeuroImage 101, 21–34.

Bell, A.J., Sejnowski, T.J., 1995. An information-maximization approach to blind separation and blind deconvolution. Neural Comput. 7, 1129–1159.

Biswal, B., Yetkin, F.Z., Haughton, V.M., Hyde, J.S., 1995. Functional connectivity in the motor cortex of resting human brain using echo-planar MRI. Med. Reson. Med. 34, 537–541.

Bodurka, J., Ye, F., Petridou, N., Murphy, K., Bandettini, P.A., 2007. Mapping the MRI voxel volume in which thermal noise matches physiological noise – implications for fMRI. NeuroImage 34, 542–549.

Bonmassar, G., Purdon, P.L., Jääskeläinen, I.P., Chiappa, K., Solo, V., Brown, E.N., Belliveau, J.W., 2002. Motion and ballistocardiogram artifact removal for interleaved recording of EEG and EPs during MRI. NeuroImage 16, 1127–1141.

Cox, R.W., 1996. AFNI: software for analysis and visualization of functional magnetic resonance neuroimages. Comput. Biomed. Res. 29, 162–173.

Cox, R.W., Hyde, J.S., 1997. Software tools for analysis and visualization of fMRI data. NMR Biomed. 10, 171–178.

Cox, R.W., Jesmanowicz, A., 1999. Real-time 3D image registration for functional MRI. Magn. Reson. Med. 42, 1014–1018.

Delorme, A., Makeig, S., 2004. EEGLAB: an open source toolbox for analysis of single-trial EEG dynamics including independent component analysis. J. Neurosci. Methods 134, 9–21.

Friston, K.J., Ashburner, J., Frith, C.D., Poline, J.B., Heather, J.D., Frackowiak, R.S.J., 1995. Spatial registration and normalization of images. Hum. Brain Mapp. 2, 165–189.

Friston, K.J., Williams, S., Howard, R., Frackowiak, R.S.J., Turner, R., 1996. Movement-related effects in fMRI time-series. Magn. Reson. Med. 35, 346–355.

Friston, K.J., 2005. Models of brain function in neuroimaging. Annu. Rev. Psychol. 56, 57–87.

Glover, G.H., Li, T.Q., Ress, D., 2000. Image-based method for retrospective correction of physiological motion effects in fMRI: RETROICOR. Magn. Reson. Med. 44, 162–167.

Gotts, S.J., Saad, Z.S., Jo, H.J., Wallace, G.L., Cox, R.W., Martin, A., 2013. The perils of global signal regression for group comparisons: a case study of Autism Spectrum Disorders. Front. Hum. Neurosci. 7 (Article 356).

Hajnal, J.V., Myers, R., Oatridge, A., Schwieso, J.E., Young, I.R., Bydder, G.M., 1994. Artifacts due to stimulus correlated motion in functional imaging of the brain. Magn. Reson. Med. 31, 283–291.

Jiang, A., Kennedy, D.N., Baker, J.R., Weisskoff, R.M., Tootell, R.B.H., Woods, R.P., Benson, R.R., Kwong, K.K., Brady, T.J., Rosen, B.R., Belliveau, J.W., 1995. Motion detection and correction in functional MR imaging. Hum. Brain Mapp. 3, 224–235.

Jo, H.J., Gotts, S.J., Reynolds, R.C., Bandettini, P.A., Martin, A., Cox, R.W., Sadd, Z.S., 2013. Effective preprocessing procedures virtually eliminate distance-dependent motion artifacts in resting state fMRI. J. Appl. Math. 935154 (2013).

Lowe, M.J., Mock, B.J., Sorenson, J.A., 1998. Functional connectivity in single and multislice echoplanar imaging using resting-state fluctuations. NeuroImage 7, 119–132.

Makeig, S., Jung, T.P., Bell, A.J., Ghahremani, D., Sejnowski, T.J., 1997. Blind separation of auditory event-related brain responses into independent components. Proc. Natl. Acad. Sci. U. S. A. 94, 10979–10984.

Mantini, D., Perrucci, M.G., Cugini, S., Ferretti, A., Romani, G.L., Del Gratta, C., 2007. Complete artifact removal for EEG recorded during continuous fMRI using independent component analysis. NeuroImage 34, 598–607.

Masterton, R.A.J., Abbott, D.F., Fleming, S.W., Jackson, G.D., 2007. Measurement and reduction of motion and ballistocardiogram artefacts from simultaneous EEG and fMRI recordings. NeuroImage 37, 202–211.

McMenamin, B.W., Shackman, A.J., Maxwell, J.S., Bachhuber, D.R.W., Koppenhaver, A.M., Greischar, L.L., Davidson, R.J., 2010. Validation of ICA-based myogenic artifact correction for scalp and source-localized EEG. NeuroImage 49, 2416–2432.

Misaki, M., Barzigar, N., Zotev, V., Philips, R., Cheng, S., Bodurka, J., 2015. Real-time fMRI processing with physiological noise correction – comparison with off-line analysis. J. Neurosci. Methods 256, 117–121.

Mulert, C., Lemieux, L. (Eds.), 2010. EEG-fMRI: Physiological Basis, Technique, and Applications. Springer-Verlag, Berlin Heidelberg.

Power, J.D., Barnes, K.A., Snyder, A.Z., Schlaggar, B.L., Petersen, S.E., 2012. Spurious but systematic correlations in functional connectivity MRI networks arise from subject motion. NeuroImage 59, 2142–2154.

Saad, Z.S., Reynolds, R.C., Jo, H.J., Gotts, S.J., Chen, G., Martin, A., Cox, R.W., 2013. Correcting brain-wide correlation differences in resting-state fMRI. Brain Connect. 3, 339–352.

Srivastava, G., Crottaz-Herbette, S., Lau, K.M., Glover, G.H., Menon, V., 2005. ICA-based procedures for removing ballistocardiogram artifacts from EEG data acquired in the MRI scanner. NeuroImage 24, 50–60.

Satterthwaite, T.D., Elliott, M.A., Gerraty, R.T., Ruparel, K., Loughead, J., Calkins, M.E., Eickhoff, S.B., Hakonarson, H., Gur, R.C., Gur, R.E., Wolf, D.H., 2013. An improved framework for confound regression and filtering for control of motion artifact in the preprocessing of resting-state functional connectivity data. NeuroImage 64, 240–256.

Talairach, J., Tournoux, P., 1998. Co-Planar Stereotaxic Atlas of the Human Brain. Thieme Medical Publishers, New York.

Van Dijk, K.R.A., Hedden, T., Venkataraman, A., Evans, K.C., Lazar, S.W., Buckner, R.L., 2010. Intrinsic functional connectivity as a tool for human connectomics: theory, properties, and optimization. J. Neurophysiol. 103, 297–321.

Van Dijk, K.R.A., Sabuncu, M.R., Buckner, R.L., 2012. The influence of head motion on intrinsic functional connectivity MRI. NeuroImage 59, 431–438.

Zotev, V., Krueger, F., Phillips, R., Alvarez, R.P., Simmons, W.K., Bellgowan, P., Drevets, W.C., Bodurka, J., 2011. Self-regulation of amygdala activation using real-time fMRI neurofeedback. PLoS One 6, e24522.

Zotev, V., Yuan, H., Phillips, R., Bodurka, J., 2012. EEG-assisted retrospective motion correction for fMRI: E-REMCOR. NeuroImage 63, 698–712.